# Comparative Investigation of Two Random Medium Models for Concrete Mesostructure

**Shixue Liang[1], Zhongshu Xie[1] and Tiancan Huang[2, *]**

**Abstract:** Concrete is intrinsically endowed with randomness on meso-scale due to the random distribution of aggregates, mortar, etc. In this paper, two random medium models of concrete mesostructure are developed and comparative studies are provided based on random field representation approach. In the first place, concrete is considered as a kind of one-phase random field, where stochastic harmonic function is adopted as the approach to simulate the random field. Secondly, in order to represent the stochastic distribution of the multi-phase of concrete such as aggregates and mortar, two-phase random field based on the Nataf transformation and the Hermite polynomials are introduced. Then, the proposed two random medium models are testified by the multi-scale simulation results, specifically, the mean value of the homogenized stress-strain relationship and the damage evolution curve. Meanwhile, the generalized density evolution equation is utilized to measure the consistency of these two random medium models by the probability distribution of damage.

**Keywords:** Concrete, one-phase random field, two-phase random field, multi-scale.

## 1 Introduction

Due to the random distribution of constituents (aggregates, cement, etc.) and defects (micro-cracks and micro-voids) on meso-scale, concrete exhibits significant random material properties, ranging from Young's modulus, strength to softening behaviors. In order to well capture these random behaviors, there is a fundamental need for the quantitative characterization of the random mesostructure of concrete. The random modeling of the concrete is critical not only for a better understanding of the material properties, but also for the reliability assessment of concrete multi-scale modeling.

---

[1] School of Civil Engineering and Architecture, Zhejiang Sci-Tech University, Hangzhou, 310018, China.
[2] Earthquake Engineering Research & Test Centre, Guangzhou University, Guangzhou, 510006, China.
* Corresponding Author: Tiancan Huang. Email: tiancanhuang@163.com.

### 1.1 Random modeling of concrete micro-structures

There are basically three approaches on random modeling of concrete mesostructures: the digital image based approach, the random aggregate approach and the random field based approach. As for the digital image based approach, the optical devices such as X-ray scanners or CT (Computed Tomography) are applied to record the spatial distribution of the multi-phase of concrete [Nitka and Tejchman (2018); Ren, Yang, Sharma et al. (2015); Yang, Ren, Sharma et al. (2017)]. The digital images can be separated into aggregate phase and mortar phase by different gray values. Distinct material properties are assigned for the aggregates and mortar separately. Admittedly, the image based approach provides a relatively accurate and realistic way to model the mesostructure of concrete. However, usually a small number of samples can be obtained due to the high costs of the experimental and reconstructive process. Therefore, the reconstructed samples of the concrete could be inadequate from the statistical point of view. Partially stemming from the image based approach, the random aggregate approach scatters random distributed fully graded aggregates in the matrix to represent the mortar. By mapping three-dimensional (3D) aggregates into two-dimensional (2D) shapes, circular [Ma, Xu and Li (2016)], quadrangular [Li, Yu, Cao et al. (2018)] as well as polygonal [Ma, Song and Xu (2018)] aggregate can be generated.

According to the development of random field theory, spatial correlated random material properties of concrete, such as Young's modulus, strength or fracture energy can be generated as random field. Bruggi et al. [Bruggi, Casciati and Faravelli (2008)] generated three non-Gaussian, multivariate and correlated random fields for the modeling of the Young's modulus, tensile strength and fracture energy, respectively. Within the context of finite element, the random fracture phenomenon is validated by Monte Carlo simulation. Yang et al. [Yang and Xu (2008); Yang, Su, Chen et al. (2009)] simulated random cracking process by considering a 2D Weibull distributed random field of tensile strength. Moreover, the method was expanded into 3D Weibull random field of tensile strength in simulating the realistic crack patterns in concrete like heterogeneous quasi-brittle material [Su, Yang and Liu (2010)]. Liang et al. [Liang, Ren and Li (2013)] applied a stochastic harmonic function based random field to simulate the damage process and failure modes of concrete.

For the simplification of random field reconstruction, the aforementioned random field based models are inclined to deem concrete as one-phase random field. When taking a close observation at the concrete, it is evident to find out that the material properties ranging from strength to fracture energy of aggregates are much stronger than that of mortar, usually reach as high as three times in the regular concrete [Neville (1995)]. Through the experimental observation, it is also validated that the cracks mainly happen in the mortar phase or the interface between aggregates and mortar. Hence, it is more reasonable to consider the concrete as two- or multi-phase random medium. A number of approaches have been proposed to address the reconstruction of two/multi-phase random fields [Feng, Cen, Li et al. (2016); Ilango, Sarkar and Sameen (2013)]. The primary idea

of these approaches is that once the intermediate Gaussian field has been generated, the generation of two-phase random field can be done conveniently using a variety of existing simulation methods, such as Nataf transformation. The two-phase random field reconstruction methods have been adopted to the permeability and conductivity of sandstones and porous soil. Although the two-phase random field is particularly suitable for the random modeling of concrete, to the best knowledge of the authors, there is seldom application on the fracture or damage modeling of concrete microstructure to date. Therefore, one of the prospective of this work is to apply the two-phase random field to the meso-scale modeling of concrete.

## 1.2 Multi-scale modeling approach

Multi-scale modeling techniques provide effective ways to evaluate how the random material properties on micro- or meso-scale influence the macroscopic material behaviors. The reconstructed random mesostructure could also be testified by the multi-scale simulation results. Guedes et al. [Guedes and Kikuchi (1990)] attained the effective elastic parameters of the composite materials by homogenization method with adaptive finite element. Fish et al. [Fish and Yu (2001)] introduced a multi-scale damage model based on the asymptotic homogenization. Ren et al. [Ren, Chen, Li et al. (2011)] proposed a micro-crack informed damage model, where the Helmholtz free energy bridging is deduced and utilized as the vehicle to relate the cracked micro-structure to damaged macro-scale continua.

As for the random materials, multi-scale modeling is also thriving recently. Taking randomly distributed grains into consideration, Wriggers et al. [Wriggers and Moftah (2006)] developed a multi-scale damage model from meso-scale analysis, in which the size of aggregates is Fuller distributed and the location of the aggregates is uniformly distributed. Benedetti et al. [Benedetti and Aliabadi (2013)] proposed a multi-scale damage model for a polycrystalline quasi-brittle material. Lin et al. [Lin, Chen and Liang (2016)] performed micro-crack informed multi-scale analysis to consider the failures of material with stochastic microstructure. Based on the multi-scale damage representation, Liang et al. [Liang, Chen, Li et al. (2017)] investigated the relationship of the statistical variation of microscopic concrete properties and macroscopic statistical variations.

## 1.3 Scope of this study

This paper presents a comparative study of two random medium models of concrete mesostructure under the framework of multi-scale modeling. Another objective of this study is to explore how the random mesostructure affects the probability distribution of macroscopic material properties. The paper is organized as follows. In Section 2, two random medium models are put forward. As for the one phase random medium model, the material property of concrete is assumed as Gaussian random field by stochastic harmonic function. As for the two-phase random field reconstruction, the aggregate is considered as the strong phase, while the mortar is considered as the weak phase. In Section 3, the homogenization based multi-scale energy bridging is applied as the

framework so that macroscopic stress-strain relationship as well as damage evolution can be attained from the meso-scale analysis. Then, the numerical model of mesoscopic concrete based on the cohesive element and finite element with respect to the irregular cracking process is given in Section 4. Comparisons between one-phase random medium model and two-phase random medium model are given by macroscopic stress-strain relationship. The generalized density evolution equation (GDEE) is introduced to further compare the probability density function (PDF) of the damage based on these two random medium models. Discussion and Concluding remarks are given in Section 5.

## 2 Two random medium models

### 2.1 One phase random medium model

In the one phase random medium model, the sizes and structures of different phases are represented by the spatial correlation relationship of the random field, hence the specific phases like aggregates and mortar are not explicitly shown in this approach.

A 2D Gaussian random field $Y_0(x_1, x_2)$ with zero mean value ($\mu=0$) and unit standard deviation ($\beta=1$) is generated by the newly developed stochastic harmonic function (SHF). Substantially, SHF belongs to the family of spectrum representation, whereas only finite stochastic harmonic functions [Chen, Sun, Li et al. (2013)] are required for the prescribed target power spectral density function.

The SHF of 2D random field is

$$Y(x_1, x_2)$$
$$= \sqrt{2} \sum_{n_1=1}^{N_1} \sum_{n_2=1}^{N_2} \left[ A_{n_1 n_2} \cos(K_{1n_1} x_1 + K_{2n_2} x_2 + \Phi_{n_1 n_2}^{(1)}) + \tilde{A}_{n_1 n_2} \cos(K_{1n_1} x_1 - K_{2n_2} x_2 + \Phi_{n_1 n_2}^{(2)}) \right] \quad (1)$$

where $Y(x_1, x_2)$ is the reconstructed random field for $Y_0(x_1, x_2)$; $N_1$, $N_2$ are the number of the components; $A_{n_1 n_2}$, $\tilde{A}_{n_1 n_2}$ represent the amplitudes of the $n_1$-th harmonic components; $K_{1n_1}$, $K_{2n_2}$ denote the corresponding wave numbers; $\Phi_{n_1 n_2, 1}$, $\Phi_{n_1 n_2, 2}$ are independent random phases. Defining the cut-off wave numbers $K_{1u}$ and $K_{2u}$, the whole support of $K_{1n_1}$ and $K_{2n_2}$ should be $[0, K_{1u}]$ and $[0, K_{2u}]$, respectively. The interval points $K_{1n_1}^{(p)}$ ($1 \leq n_1 \leq N_1 - 1$) meet the criterion that $0 \leq K_{11}^{(p)} \leq K_{12}^{(p)} \leq \ldots \leq K_{1N_1-1}^{(p)} \leq K_{1u}$, where $K_{10}^{(p)}=0$, $K_{1N_1}^{(p)}=K_{1u}$. Similarly, the interval points $K_{2n_2}^{(p)}$ ($1 \leq n_2 \leq N_2 - 1$) have $0 \leq K_{21}^{(p)} \leq K_{22}^{(p)} \leq \ldots \leq K_{2N_2-1}^{(p)} \leq K_{2u}$, where $K_{20}^{(p)}=0$, $K_{2N_2}^{(p)}=K_{2u}$.

$K_{1n_1}$, $K_{2n_2}$, $\Phi_{n_1 n_2, 1}$, $\Phi_{n_1 n_2, 2}$ are random variables in Eq. (1), and the harmonic conditions should be adopted:

(i) $K_{1n_1}$, $K_{2n_2}$ ($n_1=1, 2, \ldots, N_1$, $n_2=1, 2, \ldots, N_2$) are independent random variables, which follow a uniform distribution over the sub-supports as

$$p_{K_{jnj}}(K_j)=\begin{cases} \dfrac{1}{K^{(p)}_{jn_j}-K^{(p)}_{jn_j-1}}=\dfrac{1}{\Delta K_{jn_j}}, & K\in\left(K^{(p)}_{jn_j-1},K^{(p)}_{jn_j}\right], \quad j=1,2 \\ 0, & \text{other} \end{cases} \tag{2}$$

(ii) $\Phi_{n_1n_2,1}$, $\Phi_{n_1n_2,2}$ are independent random variables which are uniformly distributed in the range of $[0,2\pi]$;

(iii) $A_{n_1n_2}$, $\tilde{A}_{n_1n_2}$ can be calculated by the following equations

$$A_{n_1n_2}=\sqrt{2S_{Y_0Y_0}(K_{1n_1},K_{2n_2})\Delta K_{1n_1}\Delta K_{2n_2}} \tag{3}$$

$$\tilde{A}_{n_1n_2}=\sqrt{2S_{Y_0Y_0}(K_{1n_1},-K_{2n_2})\Delta K_{1n_1}\Delta K_{2n_2}} \tag{4}$$

where $S_{Y_0Y_0}$ is the power spectrum density (PSD) of the target random field.

The relationship between correlation function and PSD is given by Fourier transform as

$$S_{Y_0Y_0}(K_1,K_2)=\frac{1}{(2\pi)^2}\int_{-\infty}^{\infty}\int_{-\infty}^{\infty}R_{Y_0Y_0}(\xi_1,\xi_2)e^{-i(K_1\xi_1+K_2\xi_2)}d\xi_1d\xi_2 \tag{5}$$

where $R_{Y_0Y_0}$ is the autocorrelation function of the target random field; $\xi_1$, $\xi_2$ are the distance of $x_1$, $x_2$ directions.

If the autocorrelation function of random field is prescribed, the procedure to reconstruct the random filed $Y(x_1,x_2)$ can be summarized as follows:

1. Specify the cut-off wave number $K_{1u}$,$K_{2u}$ and separate the whole support $[0,K_{1u}]$ and $[0,K_{2u}]$ into $\left[K^{(p)}_{jn_j-1},K^{(p)}_{jn_j}\right]$ s.
2. Take steps (i) and (ii) for the random parameters in SHFs.
3. Generate samples by Eq. (1) where the involved amplitudes are obtained by Eqs. (3) and (4).

A thorough investigation is proposed that the random field generated by SHFs are stationary and asymptotically Gaussian [Chen, Sun, Li et al. (2013)].

As for any Gaussian random field $Y_1(x_1,x_2)$ with non-zero mean ($\mu\neq0$) and non-unit standard deviation ($\beta\neq1$), the following relationship should be applied as

$$Y_1(x_1,x_2)=\mu+\beta^2Y(x_1,x_2) \tag{6}$$

### 2.2 Two phase random medium model

To start with, we consider concrete as two phase random field: the strong phase which indicates the aggregates in it and the weak phase which indicates the mortar and other components. A discrete valued random field can be demonstrated below to simulate the concrete as:

$$Z_0(\boldsymbol{x}) = \begin{cases} A & \text{if x in the strong phase} \\ B & \text{if x in the weak phase} \end{cases} \tag{7}$$

where $\boldsymbol{x} = \{x_1, x_2\}$ is the 2D coordinate for the simplicity.

Assuming that the strong phase represents the aggregate of concrete and weak phase represents the mortar, it is obvious that A's have a probability equal to the ratio of aggregates, which can be given as '$\rho$', and B's have a probability $(1 - \rho)$. The ratio of aggregates can be calculated by mix proportion of concrete.

Normalize the random field $Z_0(\boldsymbol{x})$ into $\mu=0$, $\beta=1$ and define the random field $Z(\boldsymbol{x})$ as follows:

$$Z(\boldsymbol{x}) = \begin{cases} \dfrac{\rho - 1}{\sqrt{\rho(1 - \rho)}} & \text{if x in the strong phase} \\ \dfrac{\rho}{\sqrt{\rho(1 - \rho)}} & \text{if x in the weak phase} \end{cases} \tag{8}$$

The autocorrelation function of the normalized random field yields

$$\begin{aligned} R_{ZZ}(\boldsymbol{x}, \boldsymbol{x}') &= E[Z(\boldsymbol{x})Z(\boldsymbol{x}')] \\ &= \int_{-\infty}^{\infty} \int_{-\infty}^{\infty} z_1 z_2 p_{zz}(z_1, z_2) dz_1 dz_2 \end{aligned} \tag{9}$$

where $p_{zz}(z_1, z_2)$ indicates the bivariate discrete distribution of $Z$.

The Nataf transformation is then used to convert the Gaussian random field $Y$ which can be generated by SHFs into the normalized two-phase random field $Z$. The autocorrelation function of $Z$ are used to compute the autocorrelation function of $Y$. Nataf transformation holds that a certain $Z$ value 'z' can be mapped to a $Y$ value 'y' under the same cumulative distribution functions (CDF). Therefore, the mapping between $Z$ and $Y$ is

$$F_Z(z) = F_Y(y) \tag{10}$$

where $F_Z(z)$ and $F_Y(y)$ denote the CDF of discrete random variable of $z$ and Gaussian random variable $y$, respectively. This Nataf transformation is demonstrated in Fig. 1.

It is clearly demonstrated in Fig. 1 that the CDF of normalized $Z$ is step like where the probability of $\rho$ represents the strong phase (aggregates) and the probability of $(1 - \rho)$ represents the weak phase (mortar). Take Eq. (10) into consideration that the region $y \leq y_1$ can be mapped as the strong phase and the region $y > y_1$ can be mapped as the weak phase.
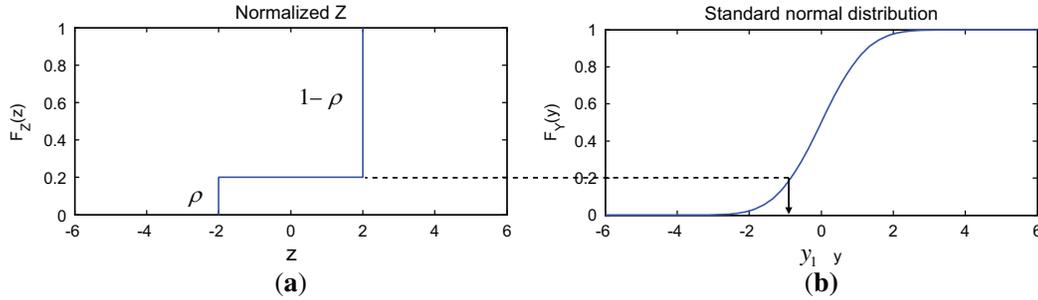
**Figure 1:** Nataf tranformation. (a) Normalized Z. (b) Standard Gaussian distribution

Therefore, the Nataf transformation is represented as

$$t(y) = \begin{cases} \dfrac{\rho - 1}{\sqrt{\rho(1-\rho)}} & y \leq y_1 \\[3mm] \dfrac{\rho}{\sqrt{\rho(1-\rho)}} & y > y_1 \end{cases} \tag{11}$$

Substituting Eq. (11) into Eq. (9), it yields

$$\begin{aligned} R_{ZZ}(\boldsymbol{x},\boldsymbol{x}') &= E[t(Y(\boldsymbol{x})) \cdot t(Y(\boldsymbol{x}'))] \\ &= \int_{-\infty}^{\infty} \int_{-\infty}^{\infty} t(y_1)t(y_2)p_{tt}(y_1,y_2)dy_1 dy_2 \end{aligned} \tag{12}$$

where $p_{tt}(y_1, y_2)$ is the bivariate Gaussian distribution.

The Hermite polynomials is applied to solve Eq. (12) as

$$p_{tt}(y_1,y_2) = \sum_{i=0}^{\infty} \sum_{j=0}^{\infty} c_{ij} H_i(y_1) H_j(y_2) \phi(y_1) \phi(y_2) \tag{13}$$

where $\phi(x) = e^{-x^2/2}/\sqrt{2\pi}$ is the Gaussian probability distribution function; $c_{ij}$ is the shape function which can be obtained by orthogonal condition Hermite polynomials.

Substituting Eq. (13) into Eq. (12), the following relationship between $R_{YY}$ and $R_{ZZ}$ can be calculated (see [Ilango, Sarkar and Sameen (2013)] for details) as

$$R_{ZZ} = \sum_{m=0}^{\infty} \frac{G_m^2}{m!} R_{YY}^m \tag{14}$$

$$G_m = \int_{-\infty}^{\infty} t(y) H_m(y) \phi(y) dy \tag{15}$$

With the prescribed ratio of aggregates $\rho$ and autocorrelation function $R_{ZZ}$, the procedure to generate the random filed $Z_0$ can be summed up as follows:

1. Calculate $R_{YY}$ of the Gaussian random field through Eqs. (14) and (15).
2. Generate the samples of Gaussian random field by SHF based on Eq. (1) where the relevant parameters are from (i), (ii), Eqs. (3) and (4).
3. Convert the samples of Gaussian random field into normalized two-phase random field $Z$ by using Eq. (11).
4. Transform $Z$ into $Z_0$ by assigning the value of $A$ and $B$ in Eq. (7) to the corresponding phase in Eq. (8).

The detailed generation process and the samples of the one- and two-phase random field are given in Section 4.

## 3 Multi-scale modelling of concrete

As for the concrete, it is conventionally treated as a homogeneous material on macro-scale, while the heterogeneities and randomness in concrete micro-structures (aggregates, cement, etc.) strongly influence the macroscopic material properties. Therefore, the multi-scale modeling is required to solve complex problems which involve the micro-structure of material.

It should be mentioned that although the randomness is considered in meso-cell, the multi-scale problems is solved by the approximated assumption of the representative volume element (RVE) and the homogenization based damage representation. As the foundation of the homogenization, the RVE is defined clearly in two situations: (1) the micro- or meso-cell of the material is periodic; (2) the micro- or meso-cell contains sufficient numbers of the micro-scale element that process the statistical periodicity and ergodicity. Ostoja-Starzewski [Ostoja-Starzewski (2006)] clarified the criterion of the random material, in which the stochastic representative volume element (SRVE) can be transferred into RVE. Meanwhile, the RVE can only be approached approximately on finite scales when the meso-cell is stochastic. In this study, the approximated assumption of the RVE is considered as the cornerstone of homogenization based multi-scale damage representation.

Considering a two-scale problem, the macroscopic coordinate and the mesoscopic coordinate x are adopted. In this study, it should be noted that the meso-scale coordinate $x$ is the same as the random field of concrete microstructure. The relationship between $x$ and $w$ could be defined by introducing a small scale parameter $\lambda$ as

$$w = \frac{x}{\lambda} \tag{16}$$

As demonstrated in Fig. 2, a 2D domain $\Omega$ and its boundary $\Gamma$ is considered at macro-scale. Taking a small region of $\Omega$ into consideration, it can be represented as a random meso-cell $\Omega_x$ which contains a distribution of arbitrary micro-cracks $\Gamma_c$. In the two-scale problem, $\boldsymbol{\sigma}$ is
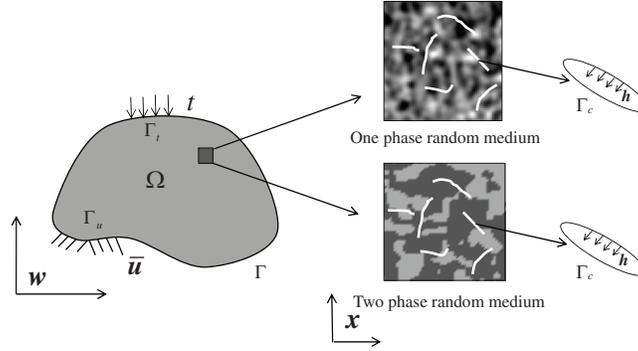
**Figure 2:** Two scale problem

the stress in which mesoscopic and macroscopic responses are embedded in the total solution; $n$ is the normal vector of surface; $u$ is the displacement; $\bar{u}$ is the prescribed displacement on the surface $\Gamma_u$; $t$ is the surface traction on $\Gamma_t$ and $h$ is the surface traction on $\Gamma_c$.

As shown in Fig. 3, the homogenized stress and strain of meso-cell actually represent the macroscopic stress and strain since the same homogenous assumptions are made.

The homogenized stress and strain are defined as the results of the tractions and displacements prescribed on the homogeneous material with the following definition as

$$\bar{\sigma}=\frac{1}{V_x}\oint_{\partial\Omega_x}(t\otimes x)\mathrm{d}\Omega \tag{17}$$

$$\bar{\varepsilon}=\frac{1}{2V_x}\oint_{\partial\Omega_x}(u\otimes n+n\otimes u)\mathrm{d}\Gamma \tag{18}$$

Accordingly, define the averaged stress and strain which represent the averaged stress and strain in meso-cell as

$$\langle\sigma\rangle=\frac{1}{V_x}\int_{\Omega_x}\sigma\mathrm{d}\Omega \tag{19}$$

$$\langle\varepsilon\rangle=\frac{1}{V_x}\int_{\Omega_x}\varepsilon\mathrm{d}\Omega \tag{20}$$

After the definition of both the homogenized and averaged stress and strain, the main perspective is to attain the homogenized stress and strain, namely the macroscopic stress and strain from the meso-cell analysis.
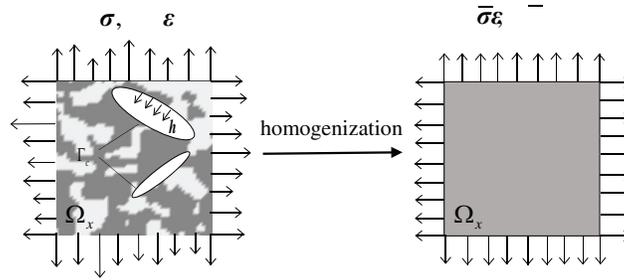
**Figure 3:** Homogenization procedure

As widely applied in damage models [Ju (1989); Wu, Li and Faria (2006)], Helmholtz free energy (HFE) is employed to relate the strain energy in the cracked mesostructure and the damaged homogenized continuum.

The HFE of the meso-cell is defined as

$$\psi = \frac{1}{2}\boldsymbol{\sigma} : \boldsymbol{\varepsilon} \tag{21}$$

The homogenized HFE evolves as

$$\bar{\psi} = \frac{1}{2}\bar{\boldsymbol{\sigma}} : \bar{\boldsymbol{\varepsilon}} \tag{22}$$

The relationship between the HFE of the homogenized material to the HFE [Ren, Chen, Li et al. (2011)] in the cracked micro-structure is provided as

$$\bar{\psi} = \frac{1}{V_x}\left(\int_{\Omega_x} \psi \, \mathrm{d}\Omega + \frac{1}{2}\oint_{\Gamma_c} \boldsymbol{u} \cdot \boldsymbol{h} \, \mathrm{d}\Gamma\right) \tag{23}$$

In this study, we adopt the scalar damage model as

$$d = 1 - \frac{\bar{\psi}}{\psi_0} \tag{24}$$

where $\psi_0$ is the HFE of the undamaged material with the expression as

$$\psi_0 = \frac{1}{2}\boldsymbol{\varepsilon} : \mathrm{C}_0 : \boldsymbol{\varepsilon} \tag{25}$$

where $\boldsymbol{C}_0$ is the undamaged constitutive tensor.

In the present paper, Eq. (24) is employed to obtain the damage evolution functions for concrete materials.

## 4 Comparative analysis

The mesostructure of concrete is modelled by using the presented two random medium models. In order to testify these two random medium models, the geometry, boundary conditions and material properties are chosen according to a uniaxial test [Ren, Yang, Zhou et al. (2008)].

### 4.1 Numerical model of meso-cell

Since the initiation, development and coalescence of micro-cracks are highly irregular and random, the random cohesive model is generated to simulate the cracking process of brittle materials. As depicted in Fig. 4, each Delaunay triangle is directly modeled by a linear displacement based finite element. These elements are connected by the cohesive elements which represent the potential crack paths within the solid. In the simulation, the finite element is formulated by 3-noded plane stress element in ABAQUS, while the cohesive element is formulated by 4-noded cohesive element. The average size of the finite element is 1.0 mm and the average width of the cohesive element is 0.005 mm. The size of the specimen is 150 mm×150 mm. Therefore, the concrete specimen contents about 20000 finite element and 30000 cohesive elements.
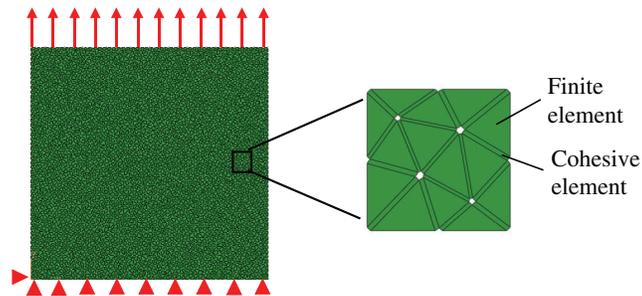


**Figure 4:** Numerical model of meso-cell

Due to the strong nonlinearities introduced by the cracking process, we choose the explicit solution algorithm to get the integration of the crack process. Since the explicit solution is applied in this simulation, the density of concrete is defined as $\rho_v$=2500 kg/m$^3$. The average time of simulation is 2.5 h for 1 sample. The numerical specimen is developed by using the finite element package in ABAQUS. According to the uniaxial tensile test, geometry of the numerical specimen and its boundary conditions are given in Fig. 4.

The fracture behaviors are described by the linear decay cohesive law [Hillerborg, Modéer and Petersson (1976)], where the cohesion on the crack tips can be solely determined by the maximum cohesive stress $f_t$ and the fracture energy $G_f$. Introduce the fracture energy as an intrinsic property of concrete, and specify its formulation as

$$G_f = \int_0^{w_1} f\,dw \tag{26}$$

where $w_1$ is the maximum width of the cracks with the expression as

$$w_1 = 2G_f/f_t \tag{27}$$

It is assumed that under shear loads, the shear fracture will happen in quasi-brittle material. As for the shear fracture (Model-II fracture), the cohesive stress can be expressed as the function of crack shear displacement (CSD). The traction-separation relationship can be defined for shear tractions and crack width. The cohesive elements in ABAQUS are based on the cohesive crack models. The material parameters such as tensile strength, shear strength, tensile (mode-I) fracture energy and shear (mode-II) fracture energy should be determined. Since the uniaxial tension is applied in this study, the shear strength and shear (mode-II) fracture energy actually doesn't play any role in the simulation. So, the shear fracture properties were simply assumed the same as the tensile ones $G_s = G_f$.

### 4.2 Generation of random medium models

Although the material properties such as Young's modulus, strength and fracture energy are random, for the simplicity and concision of the study, the elastic parameters are assumed constant. The Young's modulus and Poisson ratio are chosen as: $E = 37559$ MPa, $v = 0.2$. The tensile strength of concrete for the cohesive element is $f_t = 3.28$ MPa. In the classic fracture mechanics, the fracture energy is considered as the deterministic property of the material. However, the random cracking processes and the unpredictable failure modes cannot be well tackled by the deterministic description. In this study, the fracture energy $G_f$ is modeled as spatial correlated random field in space.

Both in the one-phase and two-phase random field, the geometry of the concrete specimen is 150 mm×150 mm (length×width) which is identical to the experimental size. The mean value of the fracture energy is chosen as $\mu = 100$ N/m, and the standard deviation of the fracture energy is $\beta = 10$ N/m.

Among various types of autocorrelation function in random field studies, exponential type [Shinozuka and Deodatis (1996)] is the mostly applied in the generation of heterogeneous materials. In this study, the autocorrelation function of random field is selected as

$$R_{ZZ}(\xi_1, \xi_2) = \exp\left(-\left(\frac{\xi_1}{b_1}\right)^2 - \left(\frac{\xi_2}{b_2}\right)^2\right), \quad 0 < \xi_1 < \infty, 0 < \xi_2 < \infty \tag{28}$$

where $b_1$, $b_2$ are the correlation lengths along $x_1$, $x_2$ directions. Since the correlation length indicates the characteristic length of a random medium, it can be chosen as maximum aggregate size in concrete according to many studies [Ren and Li (2012)]. Hence, the

correlation lengths $b_1$ and $b_2$ are chosen as $b_1=b_2=8$ mm which represent the maximum aggregate size in Ren's et al. [Ren, Yang, Zhou et al. (2008)] experiment.

The corresponding PSD can be obtained as follows

$$S_{Y_0 Y_0}(K_1, K_2) = \frac{b_1 b_2}{4\pi} \exp\left[-\left(\frac{b_1 K_1}{2}\right)^2 - \left(\frac{b_2 K_2}{2}\right)^2\right] \tag{29}$$

As for the one-phase random medium model, 100 samples of Gaussian random field are generated. The prescribed PSD and reconstructed PSD of the random field are depicted in Fig. 5. Comparisons between the target and reconstructed PSD at certain wave number are plotted in Fig. 6.



(a)                                                      (b)

**Figure 5:** PSD of one-phase random field. (a) Target PSD of one-phase random field. (b) Reconstructed PSD of one-phase random field



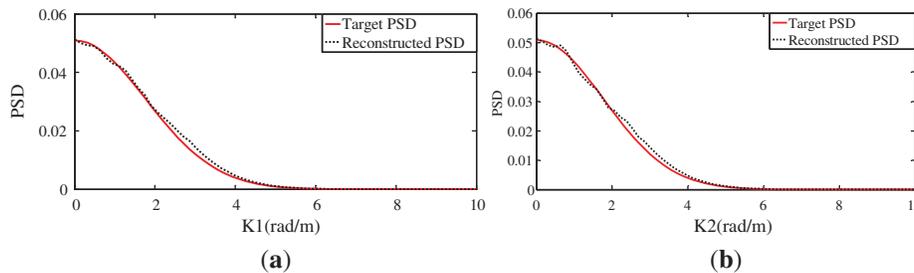(a)                                                      (b)

**Figure 6:** PSD of one-phase random field at certain wave number. (a) $K_2=0$. (b) $K_1=0$

Fig. 7 illustrates two samples of the one-phase random field. It can be seen in Fig. 7 that variation of fracture energy is within the range of $[60, 150]$ which indicates a strong variation in concrete.

According to Section 2.2, two-phase random field can be generated by Nataf transformation and Hermite polynomials where Gaussian random field is served as the intermediate random field.
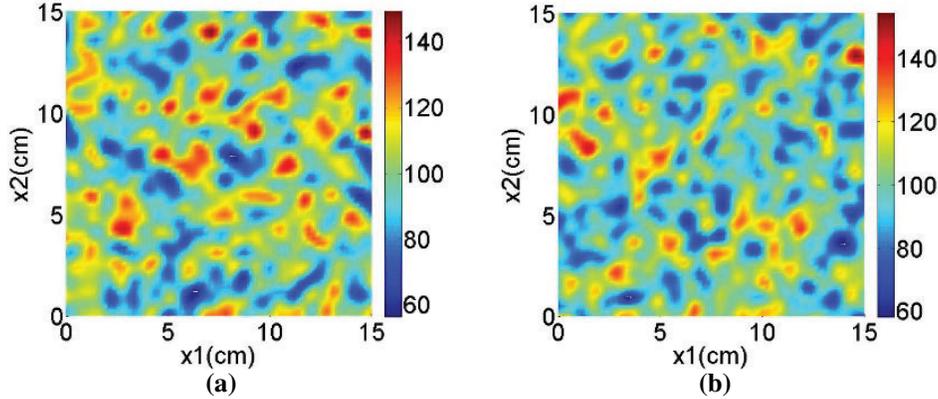
**Figure 7:** Samples of the one-phase random field. (a) Sample 1. (b) Sample 2

With the concrete mix propotion in the test, we can back-calculate the ratio of the aggregates $\rho$ as $\rho=0.451$, and the corresponding mortar as $(1-\rho)=0.549$. In this paper, the two-phase random field can be demonstrated below to simulate the concrete fracture energy as:

$$G_f(\boldsymbol{x})=\begin{cases} 157.74 \text{ N/m} & \text{if } \boldsymbol{x} \text{ is in the strong phase (aggregates)} \\ 52.58 \text{ N/m} & \text{if } \boldsymbol{x} \text{ is in the weak phase (cement)} \end{cases} \tag{30}$$

The mean value of the two-phase random field is 100 N/m, which is the same as that of one-phase random field. The correlation function $R_{ZZ}$ of the two-phase random field is also adopted as Eq. (28) where the correlation length is also $b_1=b_2=8$ mm. Then, $S_{ZZ}$ of two-phase random field can also be used as Eq. (29). The recursive adaptive Simpson quadrature is applied to solve the integration in Eq. (15). The integration interval is chosen as $[-20, 20]$. In order to achieve a balance of efficiency and accuracy, the expansion terms in Eq. (14) is given as 20 for solving $R_{YY}$.

The target PSD $S_{ZZ}$ and reconstructed PSD of the two-phase random field are depicted in Fig. 8. Similarly, 100 samples of two-phase random field are generated. Comparisons between the target $S_{ZZ}$ and the reconstructed PSD are given in Fig. 9.

Two samples are demonstrated in Fig. 10, in which the correlation length is approximated as aggregate size.
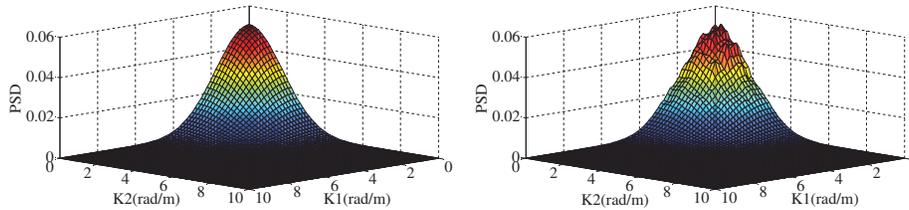


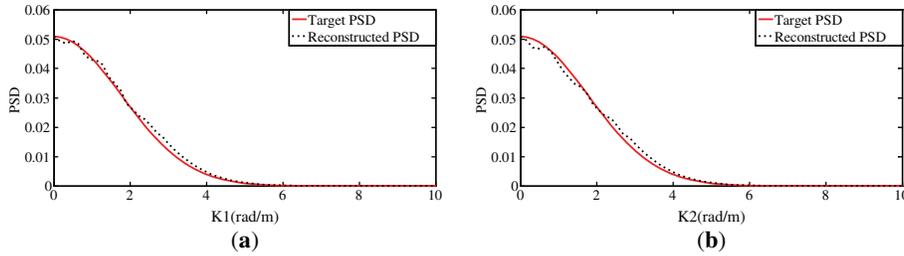**Figure 8:** PSD of two-phase random field. (a) Target PSD. (b) Reconstructed PSD

**Figure 9:** Comparisons of target and reconstructed PSD of two-phase random field. (a) $K_2=0$. (b) $K_1=0$
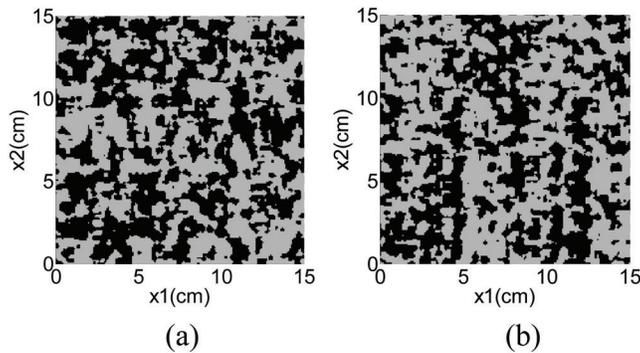


**Figure 10:** Samples of the two-phase random field. (a) Sample 1. (b) Sample 2

### 4.3 Meso-cell simulation of two random medium models

Analysis is performed on all the random samples. One of the one-phase random samples is picked for the cracking process in Fig. 11: at very early stage of loading, approximated from 0 to 0.2 $u_m$, the stress and strain both increase linearly and no micro-cracks can be observed; when the applied displacement reaches to 0.5-0.7 $u_m$, micro-cracks concentrate at a certain area and the stress concentration happens at the tips of the cracks; at final stage, a main crack cut through the concrete specimen which fits well with the experimental observations.
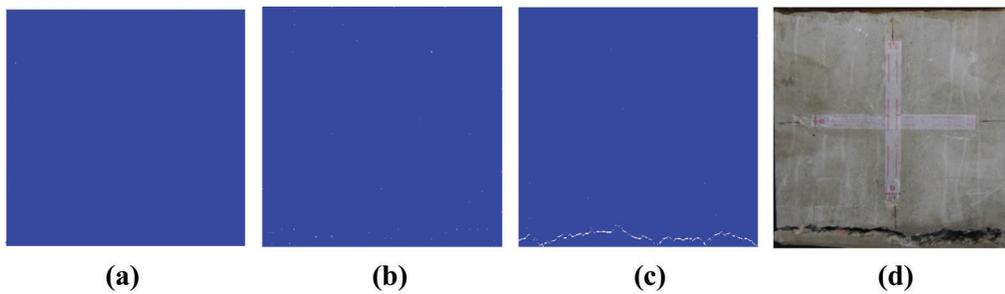


**Figure 11:** Cracking process of one-phase random sample. (a) $u=0.2$ $u_m$. (b) $u=0.7$ $u_m$. (c) $u=u_m$. (d) experimental cracks

The homogenized stress-strain relationship of 100 samples are given in Fig. 12. It can be seen from the results that the strength and the softening behavior show a strong random behavior. Comparisons between the experimental results and mean curve of stress-stain relationship are also put forward in Fig. 12(a) which validate the one-phase random medium model. The damage curves of the samples and mean curve are given in Fig. 12 (b) to directly quantify how the strength is influenced by the microscopic cracking process.
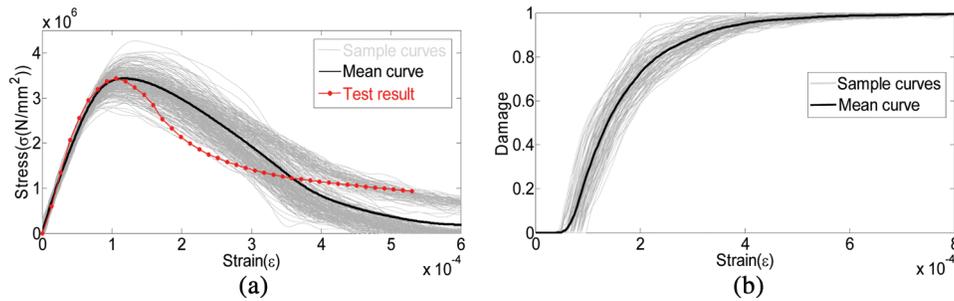


**Figure 12:** Multi-scale simulation results of one-phase random field. (a) Homogenized stress-strain curves. (b) Damage curves

Schematically, the crack propagation in a picked meso-cell at different loading stages of two-phase random medium model are shown in Fig. 13. Similar cracking process can be observed in Fig. 13 as: no micro-cracks distributed in the early stage of loading; with the increase of loading, the micro-cracks happen in a certain area of sample; in the end of loading, the micro-cracks gather together into a main crack and the tensile failure happens. Nevertheless, the cracks show more tortuousness in the two-phase random medium model than that in the one-phase random medium model. This phenomenon can be attributed to the existence of the strong phase (aggregates) which obstruct the cracking paths.
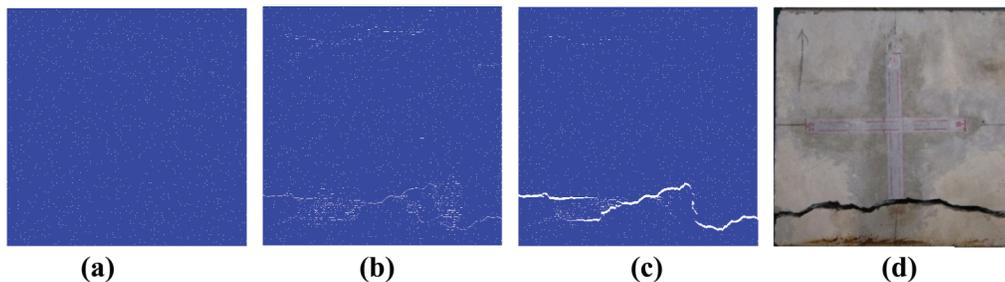


**Figure 13:** Cracking process of two-phase random sample. (a) $u=0.2\ u_m$. (b) $u=0.7\ u_m$. (c) $u=u_m$. (d) experimental cracks
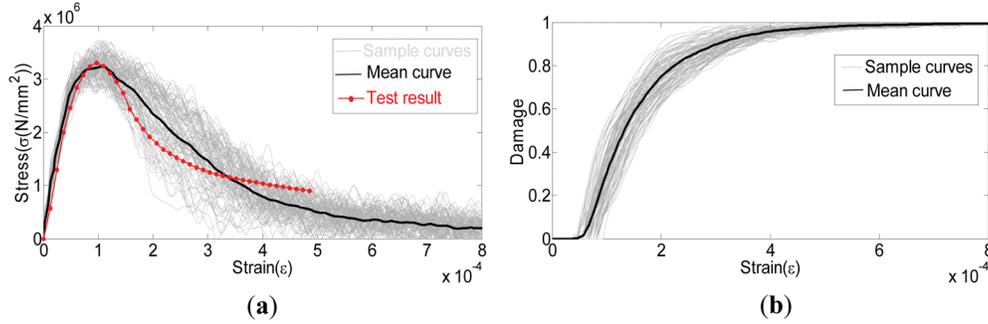
**Figure 14:** Multi-scale simulation results of two-phase random field. (a) Homogenized stress-strain curves. (b) Damage curves

Correspondingly, the homogenized stress-strain relationship of all two-phase random samples are given in Fig. 14(a). The damage curves of the samples and mean curve are given in Fig. 14(b).

### 4.4 Comparison of two random medium models

In order to quantitatively compare these two random medium models, the mean value and PDF of damage curves are investigated. The mean value of damage curves are depicted in Fig. 15.

Admittedly, it is shown in Fig. 15 that these two random medium models have similar damage curves to mean value extent. However, mean value is a relatively rough index for the random variables. Therefore, to precisely obtain probability of the homogenized stress-strain relationship and the variation in damage due to the statistical variations of microstructures, the generalized density evolution equations (GDEE) [Li and Chen (2008)] can be introduced.
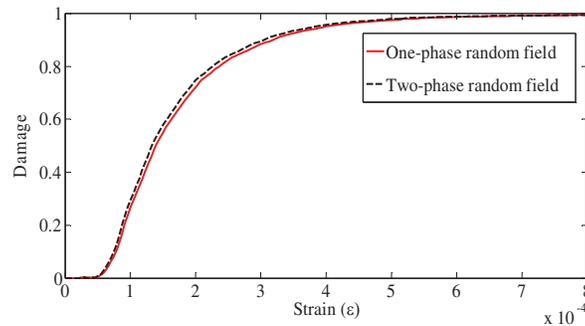


**Figure 15:** Comparison of the mean value of damage curves

In general, random damage can be represent as the function of the strain

$$d=f(\Theta,\varepsilon), \quad d(\varepsilon_0)=d_0 \tag{31}$$

where $d_0=0$ is the initial value of the damage; $\Theta$ is the random parameter vector whose joint probability density function is $p_\Theta(\boldsymbol{\theta})$ ; $\boldsymbol{\theta}$ the realization of $\Theta$. The damage rate with respect to strain is given as

$$\frac{\partial d}{\partial \varepsilon} = \frac{\partial f(\Theta, \varepsilon)}{\partial \varepsilon} = h(\Theta, \varepsilon) \tag{32}$$

The conditional transition PDF of $d$ under the condition $\{\Theta=\boldsymbol{\theta}\}$ is defined as $p_{d|\Theta}(\hat{d}, \varepsilon|\boldsymbol{\theta})$, where $d=\hat{d}$ is a realization in the probability space. The range of the possible value of damage $d$ is $0 \le \hat{d} \le 1$. When $\{\Theta=\boldsymbol{\theta}\}$, there exists $\hat{d}(\varepsilon)=f(\boldsymbol{\theta}, \boldsymbol{\varepsilon})$.

This condition can be written as

$$p_{d|\Theta}(\hat{d}, \varepsilon|\boldsymbol{\theta})=0, \quad \hat{d} \ne f(\boldsymbol{\theta}, \boldsymbol{\varepsilon}) \tag{33}$$

$$p_{d|\Theta}(\hat{d}, \varepsilon|\boldsymbol{\theta})=\infty, \quad \hat{d}=f(\boldsymbol{\theta}, \boldsymbol{\varepsilon}) \tag{34}$$

$$\int_{-\infty}^{+\infty} p_{d|\Theta}(\hat{d}, \varepsilon|\boldsymbol{\theta})d\boldsymbol{\theta}=1 \tag{35}$$

Combining Eqs. (33)-(35), the conditional transition PDF of the damage is

$$p_{d|\Theta}(\hat{d}, \varepsilon|\boldsymbol{\theta})=\delta(\hat{d}-f(\boldsymbol{\theta}, \boldsymbol{\varepsilon})) \tag{36}$$

where $\delta(\cdot)$ is the Dirac delta function.

Taking the derivative of Eq. (36), it yields

$$\begin{aligned}
\frac{\partial p_{d|\Theta}(\hat{d}, \varepsilon|\boldsymbol{\theta})}{\partial \varepsilon} &= \frac{\partial \delta(\hat{d}-f(\boldsymbol{\theta}, \boldsymbol{\varepsilon}))}{\partial \varepsilon} \\
&= \left[\frac{\partial \delta(y)}{\partial y}\right]_{y=\hat{d}-f(\boldsymbol{\theta}, \boldsymbol{\varepsilon})} \cdot \frac{\partial(\hat{d}-f(\boldsymbol{\theta}, \boldsymbol{\varepsilon}))}{\partial \varepsilon} \\
&= \frac{\partial\{\delta[\hat{d}-f(\boldsymbol{\theta}, \boldsymbol{\varepsilon})]\}}{\partial \hat{d}} \cdot \frac{\partial \hat{d}}{\partial y} \cdot \frac{\partial(\hat{d}-f(\boldsymbol{\theta}, \boldsymbol{\varepsilon}))}{\partial \varepsilon} \\
&= -h(\boldsymbol{\theta}, \boldsymbol{\varepsilon}) \cdot \frac{\partial p_{d|\Theta}(\hat{d}, \varepsilon|\boldsymbol{\theta})}{\partial \hat{d}}
\end{aligned} \tag{37}$$

Multiplying $p_\Theta(\boldsymbol{\theta})$ on both sides of Eq. (37), the GDEE for the damage evolution can be expressed as

$$\frac{\partial p_{d\Theta}(\hat{d}, \varepsilon, \boldsymbol{\theta})}{\partial \varepsilon} + h(\boldsymbol{\theta}, \boldsymbol{\varepsilon}) \cdot \frac{\partial p_{d\Theta}(\hat{d}, \varepsilon, \boldsymbol{\theta})}{\partial \hat{d}} = 0 \tag{38}$$

From Eqs. (37) and (38), the initial condition can be rewritten as

$$p_{d\Theta}(\hat{d}, \varepsilon_0, \boldsymbol{\theta}) = \delta(\hat{d} - \hat{d}_0) p_\Theta(\boldsymbol{\theta}) \tag{39}$$

Then, the PDF of $d(\varepsilon)$ is given as

$$p_d(\hat{d}, \varepsilon) = \int_{\Omega_\Theta} p_{d\Theta}(\hat{d}, \varepsilon, \boldsymbol{\theta}) \mathrm{d}\boldsymbol{\theta} \tag{40}$$

The procedure to obtain the PDF of $d(\varepsilon)$ is summarized as follows:

1. Generate one-phase and two-phase random medium samples of meso-cell given in Sections 2.1 and 2.2.
2. Simulate the cracking processes of meso-cell by cohesive elements in Section 4.1.
3. Obtain homogenized HFE by Eq. (23) and the damage evolution functions from Eq. (24).
4. Put $h(\Theta, \varepsilon) = \partial d / \partial \varepsilon$ into the generalized density evolution equation Eq. (31) and solve Eq. (37) under the initial condition Eq. (38).
5. Repeat Steps (2)-(4) for each sample and take numerical integration regarding $\boldsymbol{\theta}$ to for PDF.

The tensile damage PDFs of one-phase and two-phase random medium models are depicted in Fig. 16. Since the PDFs of tensile damage are surfaces, it is easier to show the PDF value by contour. For each strain, the PDF surface becomes the PDF curve.

In order to compare two random medium models at certain strain, PDFs at two strain $\varepsilon = 0.0002, 0.0004$ are given in Fig. 17.

It is evident in Fig. 17 that the PDFs of damage in both random medium models are irregular over an interval, especially after the peak. For a given strain configuration, the PDFs have two or more peaks, which implies the presence of bifurcations during the response process. It is noted in Fig. 17 that for a given strain, the damage PDFs of random medium models demonstrate a similar distribution.

## 5 Discussion and conclusion

### 5.1 Discussion

It can be observed in Figs. 11-17, the simulation results of one and two-phase random field have shown some similarities and distinctions. From the sample point of view, the cracking processes of one-phase and two-phase random medium are different. It is depicted in Fig. 13 that the cracking process of two-phase sample is more tortuous than the one-phase random sample in Fig. 11. However, from the homogenized stress-strain curves and damage curves point of view, these two models show similar results. These similarities are probability due to the same correlation function, mean value and variance of one-phase random field and two-phase random field, which are all collective information. The homogenization will eliminate some local behavior and retain the collective behavior. Therefore, the homogenized stress-strain curves and damage curves are similar for the one-phase and two-phase random field.
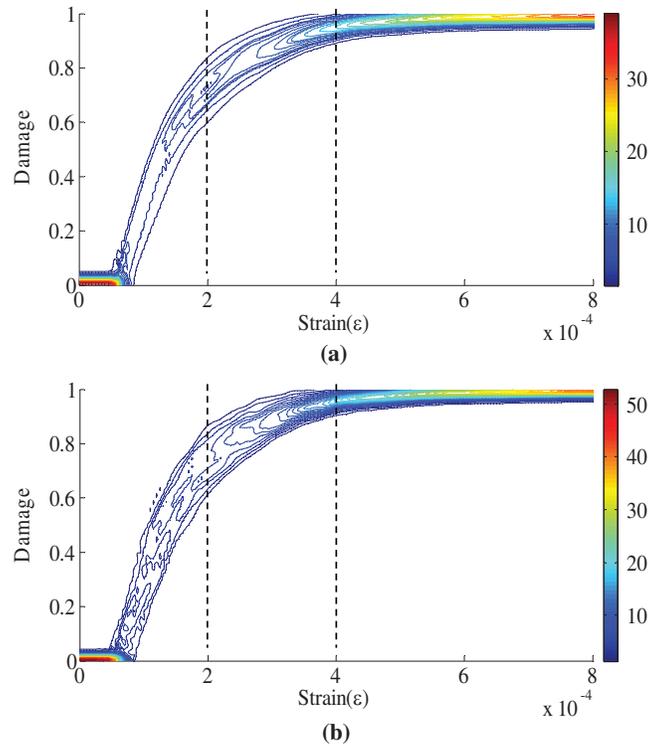
Figure 16: Comparison of the mean value of damage curves. (a) one-phase random medium. (b) two-phase random medium
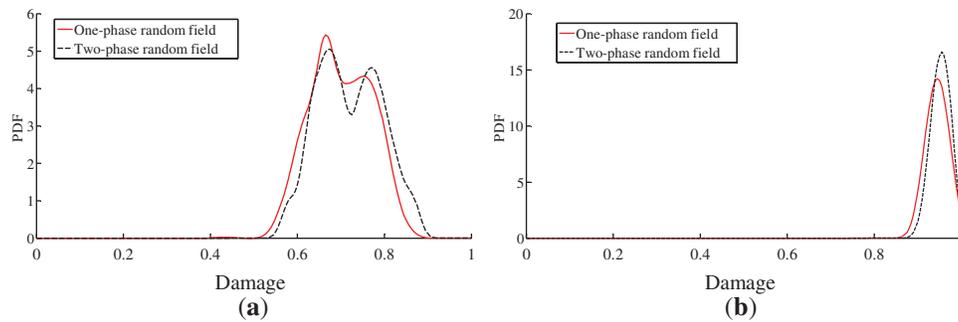


Figure 17: PDF of tensile damage curves at certain strain value. (a) $\varepsilon=0.0002$. (b) $\varepsilon=0.0004$

Accuracy and robustness of the performed analysis is influenced by the numerical methods in the meso-scale simulation, especially when fracture and damage are involved. Owing to the effectiveness and efficiency, the cohesive interface elements are employed to capture crack growth. However, the cohesive interface elements encounter several numerical

errors in some situations, such as mesh-dependencies and yield spurious crack patterns [Song, Wang and Belytschko (2008)]. These numerical errors might introduce undesired uncertainties into the subsequent statistical analysis. Therefore, the meshfree methods [Ambati, Gerasimov and De Lorenzis (2015); Bordas, Rabczuk and Zi (2008); Rangarajan, Chiaramonte, Hunsweck et al. (2015); Wei and Chen (2018)] can be applied in the meso-cell simulation to enhance the precision of the simulation.

In modeling the realistic microstructure of concrete by random field reconstruction, autocorrelation function and correlation length show significant influences on concrete samples. As for the autocorrelation function, several types such as exponential [Shinozuka and Deodatis (1996)], trigonometric [Feng, Cen, Li et al. (2016); Torquato and Yeong (1998)], chess board shaped [Ilango, Sarkar and Sameen (2013)], linear-path [Ilango, Sarkar and Sameen (2013)] are applied in the random field generation approach. Since the exponential type autocorrelation function is the most thoroughly investigated and seldom limitation has been shown in the former studies, it is also chosen in this study for the concrete microstructure. The other essential parameter in the random field modeling is the correlation length on account of determining the size and range of inhomogeneities. It is discussed in several studies [Jiao, Padilla and Chawla (2013); Simonovski, Kovač and Cizelj (2004)] that the correlation length depends upon the size of the grain, specifically the aggregate size of concrete. It is also believed by the authors that the correlation length has some connections to the characteristic length [Bazant and Pijaudier-Cabot (1989)] (internal length [Haidar, Pijaudier-Cabot, Dubé et al. (2005)]) in the nonlocal models. At the same time, however, the precise correlation length of concrete has not been issued to the best knowledge of the authors. Therefore, the maximum aggregate size is preliminarily utilized in this study. A possible direction for future work could be the deliberation of the suitable autocorrelation function as well as the correlation length in the random field modeling of concrete like multi-phase random materials.

### 5.2 Conclusion

Two random medium models of concrete based on random field reconstruction approaches are put forward in this paper. The stochastic harmonic functions are adopted for the one-phase random field, where microstructural characteristic of concrete is described by an autocorrelation function. Due to the randomly distributed aggregates, mortar and other constituents, concrete is widely accepted as a kind of multi-phase heterogeneous material. In order to represent the multi-phase microstructure of concrete, the newly developed two-phase random field generation approach is applied in this paper. The multi-scale analysis as well as the multi-scale damage representation are introduced to investigate how these two microscopic random medium models determine the macroscopic mechanical behaviors such as stress-strain relationship and damage process of concrete. It is revealed in the simulation results that fracture phenomena such as the tortuous cracks and random cracking paths, which cannot be captured in homogeneous-based models, can be well captured in this proposed random medium models. What's more, GDEE has

been introduced to thoroughly compare these two random medium models from the probability point of view. The similarities of both mean value and PDFs reveal that the presented two random medium models can be equivalently applied in the engineering problems where stress-strain relationship and damage process are the main concerns. It can also be conferred that researchers could select proper random medium model based on their research interests.

**Conflicts of Interest:** The authors declare that they have no conflicts of interest to report regarding the present study.

**References**

**Ambati, M.; Gerasimov, T.; De Lorenzis, L.** (2015): A review on phase-field models of brittle fracture and a new fast hybrid formulation. *Computational Mechanics*, vol. 55, no. 2, pp. 383-405. DOI 10.1007/s00466-014-1109-y.

**Bazant, Z. P.; Pijaudier-Cabot, G.** (1989): Measurement of characteristic length of nonlocal continuum. *Journal of Engineering Mechanics*, vol. 115, no. 4, pp. 755-767. DOI 10.1061/(ASCE)0733-9399(1989)115:4(755).

**Benedetti, I.; Aliabadi, M. H.** (2013): A three-dimensional cohesive-frictional grain-boundary micromechanical model for intergranular degradation and failure in polycrystalline materials. *Computer Methods in Applied Mechanics and Engineering*, vol. 265, no. 3, pp. 36-62. DOI 10.1016/j.cma.2013.05.023.

**Bordas, S.; Rabczuk, T.; Zi, G.** (2008): Three-dimensional crack initiation, propagation, branching and junction in non-linear materials by an extended meshfree method without asymptotic enrichment. *Engineering Fracture Mechanics*, vol. 75, no. 5, pp. 943-960. DOI 10.1016/j.engfracmech.2007.05.010.

**Bruggi, M.; Casciati, S.; Faravelli, L.** (2008): Cohesive crack propagation in a random elastic medium. *Probabilistic Engineering Mechanics*, vol. 23, no. 1, pp. 23-35. DOI 10.1016/j.probengmech.2007.10.001.

**Chen, J. B.; Sun, W. L.; Li, J.; Xu, J.** (2013): Stochastic harmonic function representation of stochastic processes. *Journal of Applied Mechanics*, vol. 80, no. 1, pp. 1-11.

**Feng, J. W.; Cen, S.; Li, C. F.; Owen, D. R. J.** (2016): Statistical reconstruction and Karhunen-Loève expansion for multiphase random media. *International Journal for Numerical Methods in Engineering*, vol. 105, no. 1, pp. 3-32. DOI 10.1002/nme.4957.

**Fish, J.; Yu, Q.** (2001): Multiscale damage modelling for composite materials: theory and computational framework. *International Journal for Numerical Methods in Engineering*, vol. 52, no. 1-2, pp. 161-191. DOI 10.1002/nme.276.

**Guedes, J.; Kikuchi, N.** (1990): Preprocessing and postprocessing for materials based on the homogenization method with adaptive finite element methods. *Computer Methods in Applied Mechanics and Engineering*, vol. 83, no. 2, pp. 143-198. DOI 10.1016/0045-7825(90)90148-F.

**Haidar, K.; Pijaudier-Cabot, G.; Dubé, J. F.; Loukili, A.** (2005): Correlation between the internal length, the fracture process zone and size effect in model materials. *Materials and Structures*, vol. 38, no. 2, pp. 201.

**Hillerborg, A.; Modéer, M.; Petersson, P.** (1976): Analysis of crack formation and crack growth in concrete by means of fracture mechanics and finite elements. *Cement and Concrete Research*, vol. 6, no. 6, pp. 773-781. DOI 10.1016/0008-8846(76)90007-7.

**Ilango, S. J. J.; Sarkar, S.; Sameen, A.** (2013): Reconstruction of 2-D porous media using Karhunen-Lóeve expansion. *Probabilistic Engineering Mechanics*, vol. 32, no. 1, pp. 56-65. DOI 10.1016/j.probengmech.2012.12.010.

**Jiao, Y.; Padilla, E.; Chawla, N.** (2013): Modeling and predicting microstructure evolution in lead/tin alloy via correlation functions and stochastic material reconstruction. *Acta Materialia*, vol. 61, no. 9, pp. 3370-3377. DOI 10.1016/j.actamat.2013.02.026.

**Ju, J. W.** (1989): On energy-based coupled elastoplastic damage theories: constitutive modeling and computational aspects. *International Journal of Solids and Structures*, vol. 25, no. 7, pp. 803-833. DOI 10.1016/0020-7683(89)90015-2.

**Li, G.; Yu, J.; Cao, P.; Ren, Z.** (2018): Experimental and numerical investigation on I-II mixed-mode fracture of concrete based on the Monte Carlo random aggregate distribution. *Construction and Building Materials*, vol. 191, no. 2, pp. 523-534. DOI 10.1016/j.conbuildmat.2018.09.195.

**Li, J.; Chen, J.** (2008): The principle of preservation of probability and the generalized density evolution equation. *Structural Safety*, vol. 30, no. 1, pp. 65-77. DOI 10.1016/j.strusafe.2006.08.001.

**Liang, S.; Chen, J.; Li, J.; Lin, S.; Chi, S. et al.** (2017): Numerical investigation of statistical variation of concrete damage properties between scales. *International Journal of Fracture*, vol. 208, no. 12, pp. 97-113. DOI 10.1007/s10704-017-0217-z.

**Liang, S. X.; Ren, X. D.; Li, J.** (2013): A random medium model for simulation of concrete failure. *Science China Technological Sciences*, vol. 56, no. 5, pp. 1273-1281. DOI 10.1007/s11431-013-5200-y.

**Lin, S.; Chen, J.; Liang, S.** (2016): A damage analysis for brittle materials using stochastic micro-structural information. *Computational Mechanics*, vol. 57, no. 3, pp. 371-385. DOI 10.1007/s00466-015-1247-x.

**Ma, H.; Xu, W.; Li, Y.** (2016): Random aggregate model for mesoscopic structures and mechanical analysis of fully-graded concrete. *Computers & Structures*, vol. 177, no. 12, pp. 103-113. DOI 10.1016/j.compstruc.2016.09.005.

**Ma, H.; Song, L.; Xu, W.** (2018): A novel numerical scheme for random parameterized convex aggregate models with a high-volume fraction of aggregates in concrete-like granular materials. *Computers & Structures*, vol. 209, no. 5, pp. 57-64. DOI 10.1016/j.compstruc.2018.08.004.

**Neville, A. M.** (1995): *Properties of Concrete*. 4th and final edition. Longman Group UK Limited, Essex.

**Nitka, M.; Tejchman, J.** (2018): A three-dimensional meso-scale approach to concrete fracture based on combined DEM with X-ray μCT images. *Cement and Concrete Research*, vol. 107, no. 5, pp. 11-29. DOI 10.1016/j.cemconres.2018.02.006.

**Ostoja-Starzewski, M.** (2006): Material spatial randomness: from statistical to representative volume element. *Probabilistic Engineering Mechanics*, vol. 21, no. 2, pp. 112-132. DOI 10.1016/j.probengmech.2005.07.007.

**Rangarajan, R.; Chiaramonte, M. M.; Hunsweck, M. J.; Shen, Y.; Lew, A. J.** (2015): Simulating curvilinear crack propagation in two dimensions with universal meshes. *International Journal for Numerical Methods in Engineering*, vol. 102, no. 3-4, pp. 632-670. DOI 10.1002/nme.4731.

**Ren, W.; Yang, Z.; Sharma, R.; Zhang, C.; Withers, P. J.** (2015): Two-dimensional X-ray CT image based meso-scale fracture modelling of concrete. *Engineering Fracture Mechanics*, vol. 133, no. 1, pp. 24-39. DOI 10.1016/j.engfracmech.2014.10.016.

**Ren, X.; Chen, J.; Li, J.; Slawson, T. R.; Roth, M. J.** (2011): Micro-cracks informed damage models for brittle solids. *International Journal of Solids and Structures*, vol. 48, no. 10, pp. 1560-1571. DOI 10.1016/j.ijsolstr.2011.02.001.

**Ren, X.; Li, J.** (2012): Dynamic fracture in irregularly structured systems. *Physical Review E*, vol. 85, no. 5, pp. 055102. DOI 10.1103/PhysRevE.85.055102.

**Ren, X. D.; Yang, W. Z.; Zhou, Y.; Li, J.** (2008): Behavior of high-performance concrete under uniaxial and biaxial loading. *ACI Materials Journal*, vol. 105, no. 6, pp. 548-557.

**Shinozuka, M.; Deodatis, G.** (1996): Simulation of multi-dimensional Gaussian stochastic fields by spectral representation. *Applied Mechanics Reviews*, vol. 49, no. 1, pp. 29-53. DOI 10.1115/1.3101883.

**Simonovski, I.; Kovač, M.; Cizelj, L.** (2004): Estimating the correlation length of inhomogeneities in a polycrystalline material. *Materials Science and Engineering: A*, vol. 381, no. 1, pp. 273-280. DOI 10.1016/j.msea.2004.04.046.

**Song, J.; Wang, H.; Belytschko, T.** (2008): A comparative study on finite element methods for dynamic fracture. *Computational Mechanics*, vol. 42, no. 2, pp. 239-250. DOI 10.1007/s00466-007-0210-x.

**Su, X. T.; Yang, Z. J.; Liu, G. H.** (2010): Monte Carlo simulation of complex cohesive fracture in random heterogeneous quasi-brittle materials: a 3D study. *International*

*Journal of Solids and Structures*, vol. 47, no. 17, pp. 2336-2345. DOI 10.1016/j. ijsolstr.2010.04.031.

**Torquato, S.; Yeong, C. L. Y.** (1998): Reconstructing random media. *Physical Review E*, vol. 57, no. 1, pp. 495-506. DOI 10.1103/PhysRevE.57.495.

**Wei, H.; Chen, J.** (2018): A damage particle method for smeared modeling of brittle fracture. *International Journal for Multiscale Computational Engineering*, vol. 16, no. 4, pp. 303-324. DOI 10.1615/IntJMultCompEng.2018026133.

**Wriggers, P.; Moftah, S. O.** (2006): Mesoscale models for concrete: homogenisation and damage behaviour. *Finite Elements in Analysis and Design*, vol. 42, no. 7, pp. 623-636. DOI 10.1016/j.finel.2005.11.008.

**Wu, J. Y.; Li, J.; Faria, R.** (2006): An energy release rate-based plastic-damage model for concrete. *International Journal of Solids and Structures*, vol. 43, no. 3, pp. 583-612. DOI 10.1016/j.ijsolstr.2005.05.038.

**Yang, Z.; Ren, W.; Sharma, R.; McDonald, S.; Mostafavi, M. et al.** (2017): In-situ X-ray computed tomography characterisation of 3D fracture evolution and image-based numerical homogenisation of concrete. *Cement and Concrete Composites*, vol. 75, no. 1, pp. 74-83. DOI 10.1016/j.cemconcomp.2016.10.001.

**Yang, Z.; Xu, X. F.** (2008): A heterogeneous cohesive model for quasi-brittle materials considering spatially varying random fracture properties. *Computer Methods in Applied Mechanics and Engineering*, vol. 197, no. 45, pp. 4027-4039. DOI 10.1016/j. cma.2008.03.027.

**Yang, Z. J.; Su, X. T.; Chen, J. F.; Liu, G. H.** (2009): Monte Carlo simulation of complex cohesive fracture in random heterogeneous quasi-brittle materials. *International Journal of Solids and Structures*, vol. 46, no. 17, pp. 3222-3234. DOI 10.1016/j.ijsolstr.2009.04.013.